

Voltage noise, multiple phase-slips, and switching rates in moderately damped Josephson junctionsMartin Žonda,¹ Wolfgang Belzig,² and Tomáš Novotný¹¹*Department of Condensed Matter Physics, Faculty of Mathematics and Physics, Charles University in Prague, Ke Karlovu 5, 121 16 Praha 2, Czech Republic*²*Fachbereich Physik, Universität Konstanz, D-78457 Konstanz, Germany*

(Received 24 October 2013; revised manuscript received 10 April 2015; published 27 April 2015)

We study the voltage noise properties including the statistics of phase-slips and switching rates in moderately damped Josephson junctions by using a novel efficient numerical approach that combines the matrix continued-fraction method with the full counting statistics. By analyzing the noise results obtained for the resistively and capacitively shunted junction (RCSJ) model we identify different dominating components; namely, the thermal noise close to equilibrium (small-current-bias regime), the shot noise of (multiple) phase-slips in the intermediate range of biases, and the switching noise for yet higher bias currents. We extract thus far inaccessible characteristic rates of phase-slips in the shot-noise regime as well as the escape and retrapping rates in the switching regime as functions of various junction parameters. The method can be extended and applied to other experimentally relevant Josephson junction circuits as well as to optical trap setups.

DOI: [10.1103/PhysRevB.91.134305](https://doi.org/10.1103/PhysRevB.91.134305)

PACS number(s): 74.40.-n, 72.70.+m, 74.78.Na, 85.25.Cp

I. INTRODUCTION

Josephson junctions (JJs) and their dynamics have been subject of intensive study ever since the discovery of the Josephson effect [1] not only because of their fascinating microscopic physical properties and high application potential but also for their ability to implement via phase dynamics elementary concepts of nonlinear dynamical systems such as chaos, multistability, and switching [2,3]. In recent years there has been progress in fabricating unconventional meso-[4,5] and nanoscopic [6] JJs exhibiting, among other effects, nonsinusoidal current-phase relations with exotic dynamics [7]. However, small junctions are more prone to the influence of environmental noise and their dynamics is inherently stochastic [8,9]. Due to the richness of dynamical regimes even the description of conventional junctions, especially in the intermediate-damping regime, may be challenging and one has to often resort to lengthy simulations [10]. It should be also mentioned that the mechanical analog of a Josephson junction, a particle in the so-called *tilted washboard potential*, can be studied by using a microparticle confined in shaped laser beams with all the dynamical properties directly optically measured [11–15]. Although such standard optical setups usually work in water in the strongly overdamped regime for the particle motion, moderately damped setups in the air or vacuum are currently being pursued [16–18]. In our presentation we stick to the JJ terminology, but one should always bear in mind the optical trapping alternative which might eventually turn out to be a more convenient platform for the experimental verification of the results (e.g., for the multiple phase-slip rates).

Another side effect of miniaturization connected to the stochastic nature of the problem is the shift of interest from just mean quantities such as the mean voltage to more elaborate statistical description including, e.g., the voltage noise in simulations [19], theory [20,21], as well as experiment [22]. In the present paper we introduce a robust and efficient numerical method based on the matrix continued-fraction (MCF) method [3] which can be used to study the voltage noise of JJs with an arbitrary level of the phase dynamics damping. The method reveals various regimes of current biasing the junction with the

corresponding dominant voltage-noise mechanisms, including thermal noise, multiple phase-slips (MPSs), and switching processes with related escape and retrapping rates whose values are easily determined. When combined with the full counting statistics (FCS) of the phase dynamics [20], it allows us to decompose (together with a clear verification mechanism, when the decomposition is legitimate) the phase dynamics into independent elementary processes [23] constituted by MPS and find their rates.

It should be stressed that MPS as well as escape and retrapping events are rather rare processes and, thus, finding their rates via direct numerical simulations is at best tedious. On the contrary, our novel numerical method gives them fairly as easily as any other stationary property, including the distribution function. Furthermore, our identification of the MPS and escape or retrapping is based on well-founded overall physical picture of a junction's dynamical behavior in the given regime (rare hopping and dichotomous processes, respectively) and gives us unambiguous answers for the rates. On the other hand, direct numerical simulations based on individual stochastic trajectories suffer from a certain degree of liberty in the definition of the relevant concepts (e.g., multiple phase-slip of a given length), which makes them even more problematic.

In this paper, for the clarity of the presentation we only introduce and demonstrate the method on the paradigmatic case of the RCSJ model with a harmonic current-phase relation. However, the numerics is directly applicable to JJs with arbitrary current-phase relations, such as in Refs. [5,24], even though the physical interpretation of the results in case of multiple nonequivalent potential minima is more complex. After a minor extension the method can be also applied to the description of the experimentally relevant circuits with structured electromagnetic environments yielding the frequency-dependent friction [9,21,25] and/or frequency-dependent voltage noise for these models. Moreover, due to the phase-charge duality, our results are also relevant for the current noise in the nanowire quantum phase-slip circuits [26]. We defer discussion of such generalizations to forthcoming presentations.

The outline of this work is the following: In Sec. II we introduce the RCSJ model and outline the matrix-continued-fraction method of its solution. In the following Sec. III we present the obtained numerical results both for the mean voltage and voltage noise quantified in terms of the appropriately defined Fano factor. We focus in more detail on the analysis of the phase-slip regime for intermediate current bias in Sec. IV and of the switching regime for large bias in Sec. V. Finally, we summarize our results and discuss their possible extensions in Sec. VI. Technical details of the MCF method are postponed to Appendix.

II. RESISTIVELY AND CAPACITIVELY SHUNTED JUNCTION MODEL & METHODS OF SOLUTION

Ideal Josephson junctions with the conventional harmonic current-phase relation $I = I_c \sin \phi$ shunted with a simple circuit environment [parallel resistance R and capacitance C ; see Fig. 1(a)] and current biased by I_b are described by the resistively and capacitively shunted junction (RCSJ) model [27]. The Langevin equations for the phase difference $\phi(t)$ and voltage $V(t) = \frac{\hbar}{2e} \frac{d\phi(t)}{dt}$ across the junction are just the first law of Kirchhoff and the Josephson voltage-phase relation:

$$I_b = I_c \sin \phi(t) + C \frac{dV(t)}{dt} + \frac{V(t)}{R} + \xi(\tau),$$

$$V(t) = \frac{\hbar}{2e} \frac{d\phi(t)}{dt}. \quad (1)$$

We can define dimensionless quantities [2] with help of the plasma frequency $\omega_p = \sqrt{2eI_c/\hbar C}$ and the quality factor of the circuit $Q = \omega_p RC \equiv \gamma^{-1}$ quantifying the level of damping of the phase dynamics as follows: junction voltage $v = \frac{QV}{I_c R}$, junction current $i = \frac{I}{I_c}$, time $\tau = \omega_p t$, temperature $\Theta = \frac{2ek_B T}{\hbar I_c}$ (with the Boltzmann constant k_B), bias current $i_b = \frac{I_b}{I_c}$, and the Gaussian white noise ζ with the correlation functions $\langle \zeta(\tau) \rangle = 0$, $\langle \zeta(\tau_1) \zeta(\tau_2) \rangle = 2\gamma \Theta \delta(\tau_1 - \tau_2)$. In

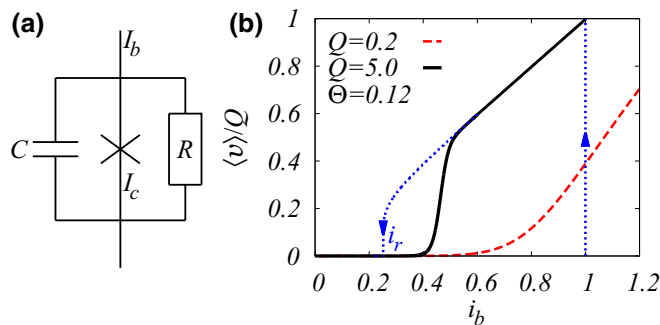


FIG. 1. (Color online) (a) Circuit representation of the RCSJ model. (b) $\langle v \rangle - i_b$ characteristics for a weakly damped junction $Q = 5$ (black solid line) and a strongly damped one $Q = 0.2$ (red dashed line). Blue dotted lines represent the hysteretic $\langle v \rangle - i_b$ characteristics for forward and backward i_b ramping of the noiseless case with $Q = 5$.

these dimensionless units the above equations (1) read

$$\frac{dv(\tau)}{d\tau} = i_b - \gamma v(\tau) - \sin \phi(\tau) + \zeta(\tau),$$

$$v(\tau) = \frac{d\phi(\tau)}{d\tau}. \quad (2)$$

This description assumes sufficiently high temperature $T \gg \hbar\omega_p/k_B$ so that quantum effects can be neglected. Equations (2) imply the associated Fokker-Planck equation [3] for the probability distribution function $W(\phi, v, \tau)$:

$$\frac{\partial}{\partial \tau} W(\phi, v; \tau)$$

$$= \left[-v \frac{\partial}{\partial \phi} + \frac{\partial}{\partial v} \left(\gamma v + \sin \phi - i_b + \gamma \Theta \frac{\partial}{\partial v} \right) \right] W$$

$$\equiv L_{\text{FP}} W(\phi, v; \tau). \quad (3)$$

We are interested in the mean voltage

$$\langle v \rangle = \int_0^{2\pi} d\phi \int_{-\infty}^{\infty} dv v W_{\text{stat}}(\phi, v), \quad (4)$$

and the (zero-frequency) voltage noise

$$S = \int_{-\infty}^{\infty} d\tau [\langle v(\tau) v(0) \rangle - \langle v(\tau) \rangle \langle v(0) \rangle] \quad (5)$$

in the stationary state $W_{\text{stat}}(\phi, v) \equiv \lim_{\tau \rightarrow \infty} W(\phi, v; \tau)$ determined by the 2π -periodic solution (in ϕ) of the equation $L_{\text{FP}} W_{\text{stat}}(\phi, v) = 0$. While the mean voltage is trivially obtained from the knowledge of the stationary probability distribution function, the computation of the voltage noise is more complicated. The general formula for the frequency-dependent voltage noise reads

$$S(\omega) = \int_{-\infty}^{\infty} d\tau e^{i\omega\tau} [\langle v(\tau) v(0) \rangle - \langle v(\tau) \rangle \langle v(0) \rangle], \quad (6)$$

and the voltage autocorrelation function can be expressed as (Ref. [3, Sec. 7.2])

$$\langle v(\tau) v(0) \rangle = \int_0^{2\pi} d\phi \int_{-\infty}^{\infty} dv v e^{|\tau| L_{\text{FP}}} v W_{\text{stat}}(\phi, v). \quad (7)$$

After introducing the convergence factors $\omega \rightarrow \omega + i0$ for $\tau > 0$ and $\omega \rightarrow \omega - i0$ for $\tau < 0$ we get

$$S(\omega) = \int_0^{2\pi} d\phi \int_{-\infty}^{\infty} dv v \left(\frac{1}{i\omega - L_{\text{FP}}} - \frac{1}{i\omega + L_{\text{FP}}} \right)$$

$$\times v W_{\text{stat}}(\phi, v). \quad (8)$$

Since we are interested in the limit $\omega \rightarrow 0$ and L_{FP} is singular (due to the existence of the stationary state), performing the limit is somewhat tricky. It can be done, however, as explained in detail in Ref. [28, Sec. IIIB], and the voltage noise can be evaluated as

$$S = -2 \int_0^{2\pi} d\phi \int_{-\infty}^{\infty} dv v R(\phi, v), \quad (9)$$

with the help of an auxiliary quantity $R(\phi, v)$ (pseudoinverse of the Fokker-Planck operator) satisfying the equation

$$L_{\text{FP}} R(\phi, v) = (v - \langle v \rangle) W_{\text{stat}}(\phi, v), \quad (10)$$

and conditions $R(\phi + 2\pi, v) = R(\phi, v)$ (periodicity) and $\int_0^{2\pi} d\phi \int_{-\infty}^{\infty} dv R(\phi, v) = 0$ [fixing one out of infinitely many solutions of Eq. (10), see Ref. [28, Sec. III E]].

We have found both $W_{\text{stat}}(\phi, v)$ and $R(\phi, v)$ numerically by the matrix continued-fraction method of Ref. [3, Sec. 11.5] which first expresses the v part of the equations in terms of quantum-oscillator-basis functions, thus obtaining a tridiagonal coupled system of ϕ -dependent differential equations (Brinkmann hierarchy). The 2π -periodic ϕ parts are then expanded into the Fourier series and solved via the MCF as explained in more detail in Appendix. The method inherently works for arbitrary current-phase relations. Furthermore, by using the finite-frequency generalization of the problem (8) (which can be further manipulated analogously to Ref. [29]), we could easily evaluate also the finite-frequency voltage noise (6).

An alternative method for evaluation of the zero-frequency voltage noise is to use the full counting statistics (FCS) approach pioneered in this context in Ref. [20]. The aim of that method is the calculation of the k -dependent (k is the counting field) cumulant generating function (CGF)

$$F(k; \tau) \equiv \ln \int_{-\infty}^{\infty} d\phi e^{ik\phi} \int_{-\infty}^{\infty} dv W(\phi, v; \tau) \quad (11)$$

from a nonstationary solution $W(\phi, v; \tau)$ of Eq. (3) (Ref. [3, Sec. 11.7]). For long times $\tau \rightarrow \infty$ the CGF generates all stationary cumulants of the voltage by derivatives with respect to k at $k = 0$ and its full k dependence can be used for evaluation of phase-slip rates, as shown below. Following the analogous derivations in Refs. [30,31], we obtain $\lim_{\tau \rightarrow \infty} F(k; \tau)/\tau = \lambda_0(k)$, where $\lambda_0(k)$ is the counting-field-dependent eigenvalue of the full problem (3) with modified boundary condition [20] $W_0(\phi + 2\pi, v) = e^{-i2\pi k} W_0(\phi, v)$ with the biggest real part [adiabatically developed with increasing k from the stationary solution $\lambda_0(k = 0) = 0$]. This eigenvalue can be also obtained by the MCF method as shown in the Appendix, Sec. A 4, and yields the mean voltage $\langle v \rangle \equiv -i\lambda_0'(0)$, voltage

noise $S \equiv -\lambda_0''(0)$, and similarly also the higher-order voltage cumulants. We have verified that both calculation methods give the same results for the mean voltage and noise.

III. RESULTS

A. $\langle v \rangle - i_b$ characteristics

In Fig. 1(b) we recapitulate for completeness the known results [3,32] for the mean voltage by plotting $\langle v \rangle - i_b$ curves for two complementary values of the quality factor representing the strongly ($Q = 0.2$) and weakly ($Q = 5$) damped cases. While the strong damping case with increasing i_b shows a smooth crossover from the nearly zero voltage (diffusive branch [9]) to the Ohmic behavior determined by R for $i_b \gtrsim 1$, the underdamped curve exhibits a much sharper transition between the two regimes. This can be understood as the noise-induced sudden switching between two coexisting dynamical states of the underdamped junction in the noiseless (zero temperature) limit represented by the dotted blue lines in the figure revealing a strong hysteresis between the forward and backward ramping of the bias current i_b . Using the above-mentioned and well-known mechanical analogy of the RCSJ model, which is the damped particle in the tilted washboard potential $U(\phi) = \cos \phi + i_b \phi$ [illustrated in the inset of Fig. 2(a)], one can easily see that the zero-voltage state (locked solution) is stable up to $i_b = 1$ while a finite-voltage state v_r (running solution) is stable down to the Q -dependent retrapping current [27] $i_r(Q) \approx 4/\pi Q \doteq 0.25$ (for the studied case with $Q = 5$) determined by the energy balance between the energy supply by the bias current and dissipation [3]. Without noise, the originally trapped ‘‘phase particle’’ stays locked in the potential minimum until the bias current is high enough to wipe off the local extremes of the potential. On the other hand, if the particle is already running then, because of the inertia, it can still overcome the local maxima and keep running if the damping is low enough. For finite temperatures the stationary $\langle v \rangle - i_b$ characteristics in the bistability region

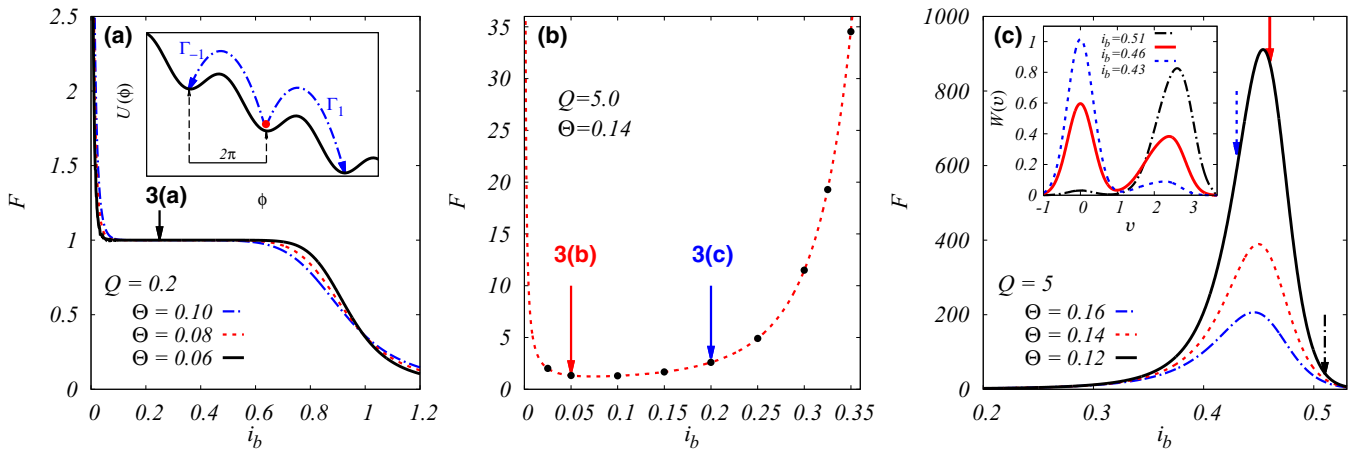


FIG. 2. (Color online) (a) Voltage-noise Fano factor for an overdamped $Q = 0.2$ and (b), (c) underdamped $Q = 5.0$ junctions and different temperatures Θ . Panel (b) depicts in detail the $\Theta = 0.14$ Fano-factor curve from panel (c) in the small- i_b regime where multiple phase-slips are the prevailing source of voltage noise. Red dashed line is the full solution calculated from the Fokker–Planck equation (3) while the overlapping black dots are the checks evaluated approximately via the MPS rates (see main text). Arrows in panels (a) and (b) refer to parameters studied in detail in the following Fig. 3. Insets show (a) mechanical analog of Eq. (2) with $\Gamma_{1 \rightarrow -1}$ being the rates of the forward and backward single phase-slips and (c) bimodal stationary distribution functions plotted for bias-current values marked with the corresponding arrows.

$i_r(Q) < i_b < 1$ is the weighted average of the running and locked solutions governed by the escape and retrapping rates, which can be determined from the noise, as demonstrated below.

B. Voltage noise

Voltage noise properties can be used to analyze the phase dynamics in far more detail. In analogy to the electronic mesoscopic transport [33,34], we conventionally express the voltage noise in terms of the dimensionless ratio called the Fano factor (see Ref. [33, p. 28]) defined as $F \equiv S(\omega = 0)/2\pi\langle v \rangle$. In Fig. 2 we plot the Fano factor for strongly damped $Q = 0.2$ (left panel) and weakly damped $Q = 5$ junctions (middle and right panels) at different temperatures. Our numerical results for the strongly damped case are very close to those for the overdamped RSJ model [20]. Because of low temperature $\Theta \ll 1$ the low-bias-current behavior for $i_b \lesssim 0.6$ can be perfectly understood by the description in terms of thermally induced forward and backward single (i.e., by 2π) phase-slips shown in the inset of the left panel. This simple picture yields for the Fano factor in this regime $F = \coth \pi i_b / \Theta$ [see Ref. [20, Eq. (28)]] exhibiting the characteristic divergence at $i_b = 0$ due to the finite thermal noise and the plateau at the Poissonian value of $F = 1$ for larger values of i_b . Above the critical current $i_b > 1$ the junction is in the running state and the prevailing component of the noise is the simple Johnson thermal noise of the resistor with $F = \Theta(2i_b^2 + 1)/(i_b^2 - 1)^{3/2}$ for $i_b \gtrsim 1 + \Theta^{2/3}$ [cf. Ref. [20, Eqs. (36) and (37)]].

The Fano factor vs bias current for the *underdamped* junction in Figs. 2(b) and 2(c) is qualitatively different from the strongly damped case. As shown in Fig. 2(b) there is also the low- i_b thermal singularity in the Fano factor followed for increasing $i_b \lesssim i_r(Q)$ by a flatter part due to multiple phase-slips discussed in previous works [9,35,36] and studied in detail below in Sec. IV. However, unlike in the overdamped case, for still-growing bias current the Fano factor rises again and becomes dominated by the strongly temperature-dependent huge peak with $F \approx 100$ to 1000 around the switching current $i_s \doteq 0.45$ [compare with Fig. 1(b)] plotted in Fig. 2(c), which is characteristic of the dichotomous switching process. This interpretation is further supported by the inset of Fig. 2(c) with the stationary voltage distribution function $W(v) \equiv \int_0^{2\pi} d\phi W_{\text{stat}}(\phi, v)$ for various bias currents showing curves with well-separated double peaks corresponding to two differently weighted metastable states. The first peak centered around $v = 0$ describes the locked phase while the second one around the i_b -dependent noiseless running solution v_r reveals the running phase. We further analyze this switching process in Sec. V.

IV. PHASE-SLIPS

Now we turn our attention to the multiple-phase-slips regime [37] with the bias current smaller than the onset of the switching regime $i_b \lesssim i_r(Q)$, as shown Fig. 2(b). Analogously to the overdamped case [20,38] the solution to the Fokker–Planck equation (3) in this regime can be approximated by a weighted sum of quasi-equilibrated sharp

($\Theta \ll 1$) Gaussian distributions around the local minima $W(\phi, v; \tau) \approx \sum_m P_m(\tau) w(\phi - 2\pi m, v)$ with [Ref. [20, Eq. (22)]]

$$w(\phi, v) = \frac{\sqrt[4]{1 - i_b^2}}{2\pi\Theta} \exp \left[-\frac{\sqrt{1 - i_b^2}}{2\Theta} (\phi - \arcsin i_b)^2 \right] e^{-\frac{v^2}{2\Theta}}, \quad (12)$$

and time-dependent weights $P_m(\tau)$. These are *assumed* to satisfy the (Markovian) master equation

$$\begin{aligned} \frac{dP_m(\tau)}{d\tau} &= \sum_{n \neq 0} \Gamma_n P_{m-n}(\tau) - \sum_{n \neq 0} \Gamma_n P_m(\tau) \\ &\equiv \sum_n \Gamma_n P_{m-n}(\tau), \text{ with } \Gamma_0 \equiv -\sum_{n \neq 0} \Gamma_n. \end{aligned} \quad (13)$$

Here, Γ_n ($n \neq 0$) are the rates of elementary MPS by $2\pi n$ [negative n corresponds to backward rates against the bias such as Γ_{-1} in the inset of Fig. 2(a)].

To find the MPS rates we use the FCS methodology introduced in Ref. [20] for the RSJ model combined with the procedure of identification of elementary processes [23]. If the master equation (13) description is a good approximation of the full phase dynamics we can evaluate the CGF from it and equate that with the full CGF calculated by the MCF as described in the last section A 4 of the Appendix. We have for the approximate probability density

$$\exp[F(k; \tau)] \approx \sum_m P_m(\tau) e^{2\pi i k m} \tilde{w}(k) \equiv \mathcal{P}(k; \tau) \tilde{w}(k), \quad (14)$$

with $\tilde{w}(k) = \exp(ik \arcsin i_b - 2\Theta k^2 / \sqrt{1 - i_b^2})$ and $\mathcal{P}(k; \tau) \equiv \sum_m P_m(\tau) e^{2\pi i k m}$ satisfying the k -dependent differential equation

$$\frac{d\mathcal{P}(k; \tau)}{d\tau} = \left(\sum_n \Gamma_n e^{2\pi i k n} - \sum_n \Gamma_n \right) \mathcal{P}(k; \tau). \quad (15)$$

This allows us to identify $\lambda_0(k) = \sum_n \Gamma_n (e^{2\pi i k n} - 1)$ in the MPS regime describing a mixture of independent Poissonian processes of phase-slips by $2\pi n$ whose rates can be evaluated as

$$\Gamma_n = \int_0^1 dk \lambda_0(k) e^{-2\pi i k n} \text{ for } n \neq 0. \quad (16)$$

Importantly, the method itself provides tools for checking its validity by comparing the approximate mean voltage $\langle v \rangle = 2\pi \sum_n \Gamma_n n$ and Fano factor $F = \sum_n \Gamma_n n^2 / \sum_n \Gamma_n n$ with those computed directly by the MCF method. In Fig. 2(b) it is explicitly shown that the two Fano factors perfectly match up to the values of i_b where the switching process sets in (and correspondence eventually breaks down).

In Fig. 3 we plot MPS rates Γ_n for strong-damping case $Q = 0.2$ [Fig. 3(a)] and weak damping case $Q = 5$; $i_b = 0.05, 0.20$ [Figs. 3(b) and 3(c)]. Only the single phase-slips are realized in the strong-damping case, which is consistent with the Fano-factor plateau at one in Fig. 2(a). The dependence of Γ_1 on i_b in the regime of the plateau is plotted in the inset with dots

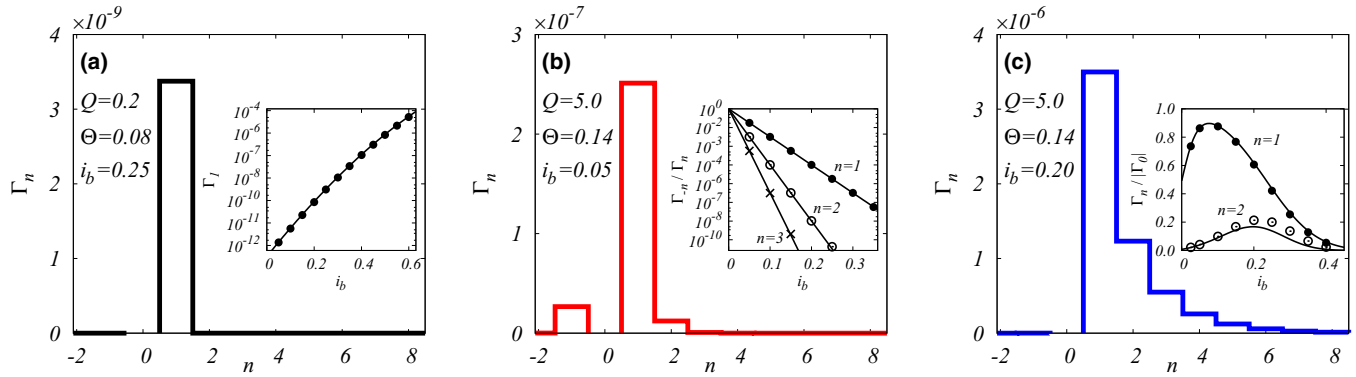


FIG. 3. (Color online) (a) Single-phase-slip rate for a strongly damped junction with $Q = 0.2$ corresponding to the unitary plateau of the Fano factor in Fig. 2(a). Inset shows comparison of the i_b dependence of the rate evaluated numerically (dots) and by the Kramers formula (17) for the overdamped case (solid line). (b), (c) Rates of MPS (of order n) for two values of the bias current i_b denoted in Fig. 2(b) by the corresponding arrows. Insets show (b) verification of the detailed balance condition and (c) a comparison of the i_b dependence of the first two normalized phase-slip rates (respective dots) with the Mel'nikov formula (lines).

and compared with the Kramers formula for escape across the adjacent barrier [20,39,40] (solid line in the inset)

$$\Gamma_e = \frac{1}{2\pi} \left(\sqrt{\frac{\gamma^2}{4} + \sqrt{1 - i_b^2}} - \frac{\gamma}{2} \right) \times \exp \left[-\frac{2 \left(i_b \arcsin i_b + \sqrt{1 - i_b^2} \right) - \pi i_b}{\Theta} \right]. \quad (17)$$

The behavior of the weak-damping case is much richer. The presence of multiple (double) phase-slips (alongside the single backward phase-slips) is evident even for small bias currents in Fig. 3(b), and their importance increases with increasing bias current [Fig. 3(c)]. The MPS rates decay slower than exponentially with increasing n especially for the bias current approaching $i_r(Q)$ and increasing Q , which is consistent with corresponding asymptotic [$i_b \rightarrow i_r(Q)$, $Q \rightarrow \infty$] results by Shushin [41]. The inset in Fig. 3(c) depicts the normalized (by $|\Gamma_0| = \sum_{n \neq 0} \Gamma_n$) rates of the single and double phase-slips as functions of i_b (dots) together with Mel'nikov's approximative asymptotic formulas [35,36] that are valid for $Q \rightarrow \infty$ (solid lines in the inset). We can see reasonable agreement which, analogously to Fig. 4 below, further improves with increasing Q (for details see the appropriate part of the next section). In the inset of Fig. 3(b) we test that the ratio $\Gamma_{-n}/\Gamma_n = \exp(-2\pi n i_b / \Theta)$ for $n = 1, 2, 3$ satisfies the detailed balance condition with the potential drop $2\pi i_b n$ along the phase-slips of the given order n .

Altogether, our method provides reliable results for the MPS rates for a wide class of junctions. Their experimental verification in the framework of JJs might be challenging though, due to the high requirements on the time resolution of the voltage pulses associated with the phase-slips. They occur (i.e., their duration is) on the timescale of the inverse plasma frequency (in the range of MHz to GHz) and their sufficient resolution (to make statistics of given multiplicities from their pulse areas) is likely to be beyond current experimental possibilities. However, one may resort here to the optical trapping setups discussed in the introduction, where the

position of the particle is continuously monitored optically and the length of the slip may be directly discerned from the position of the initial and final potential minima.

V. SWITCHING PROCESS

Finally, we analyze the regime of largest bias currents exhibiting the features of the dichotomous switching between the locked (i.e., zero voltage) and running states. Since $F \gg 1$ around the peaks in Fig. 2(c), we can neglect noise contributions inherent to the metastable states [42] and use the average voltage $\langle v \rangle$ and Fano factor F for the evaluation of the escape rate Γ_e (from locked to running state) and retrapping rate Γ_r (from running to locked state) [31]:

$$\Gamma_e = \frac{\langle v \rangle (v_r - \langle v \rangle)}{\pi v_r F}, \quad \Gamma_r = \frac{(v_r - \langle v \rangle)^2}{\pi v_r F}, \quad (18)$$

which are presented in Fig. 4 as solid lines and compared with analytical predictions (dashed lines). On one hand, switching

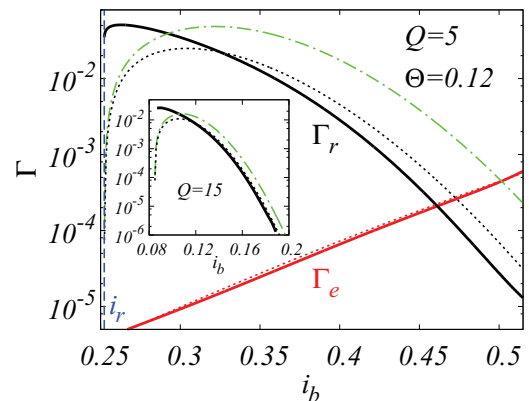


FIG. 4. (Color online) Escape rate Γ_e and retrapping rate Γ_r numerically computed from Eqs. (18) (solid lines) compared with analytical approaches (dashed lines; for details see main text). Inset shows a more detailed comparison of the numerical retrapping rate (full line) with the Mel'nikov (black dashed line) and BJMS formula (19) (green dot-dashed line) for a junction with higher quality factor $Q = 15$.

from the locked phase to the running phase happens just by thermally induced overcoming of the neighboring potential maximum and, therefore, is given by the Kramers escape rate (17) from the local potential well [40]. One can see that this prediction is in an excellent agreement with our numerical result. On the other hand, the retrapping problem is far more complicated and has not been addressed in the whole parameter regime yet, only asymptotic solutions in various limits exist.

Two different analytical approximate approaches by Ben-Jacob *et al.* [43] (BJBMS) and Mel'nikov [36,44] were introduced for the limit of very weak damping $Q \rightarrow \infty$, which yield quantitatively different result. In Fig. 4 we compare our results with those predictions for finite damping and find a rather poor agreement with either one. With increasing Q , Melnikov's approach seems to asymptotically approach our results for sufficiently large i_b , as shown in the inset. BJBMS on the other hand remains off, which might be connected with its existing critiques [44,45]. The persistent discrepancy between Melnikov's and our approach for i_b close to the onset of the bistability region is most likely caused by the breakdown of the saddle-point approximation in the root of Melnikov's method, since the locked and running states are not well separated very close to the bifurcation point in the noisy case. In any case, our numerical method presents a dramatic improvement over the existing theories. In addition, it allows to extract the retrapping rate fast and reliably in a wide range of junction parameters, in particular for arbitrary values of the quality factor Q and bias current i_b .

It might look surprising that such a discrepancy between our exact solution and the very popular BJBMS expression

$$\Gamma_r = \frac{i_b - i_r(Q)}{\sqrt{2\pi\Theta}} e^{-\frac{\varphi^2[i_b - i_r(Q)]^2}{2\Theta}} \quad (19)$$

has not been noticed before. Obviously, the wide use of formula (19) in interpretation of switching experiments such as those in Ref. [46] or in simulations such as in, e.g., Ref. [10] stems from its simple analytical form (contrary to the fairly complicated structure of Mel'nikov's result, compare Refs. [36,44]). This causes it to be used even outside of the regime of its expected validity (it was derived just in the $Q \rightarrow \infty$ limit) and despite of indications of its limitations [44,45,47]. Kautz [47] calculated the exponential part of the rate in terms of the "activation energy" and found out that it is larger than the corresponding BJBMS quantity $Q^2[i_b - i_r(Q)]^2/2$ (see Figs. 6 and 7 in Ref. [47]). This is fully consistent with our results showing that the exact retrapping rate is substantially smaller than the prediction by BJBMS.

Still, our Fig. 4 depicts that the discrepancy between the two rates for $Q = 5$ is nearly an order of magnitude. How could this escape attention in so many studies that use the BJBMS formula? When carefully analyzing works citing the original BJBMS paper (around 100), we realized that the vast majority of them uses it in some indirect way just as one of several ingredients describing a physical mechanism (for example, the issue of nonmonotonic width of switching histograms in Ref. [46]). The validity of the formula is not directly addressed and its possible shortcomings are likely to be absorbed in fitting procedure(s). In accordance with the statement in Ref. [10], we found just a *single* experimental work [48] addressing directly the retrapping process and, thus, measuring more or

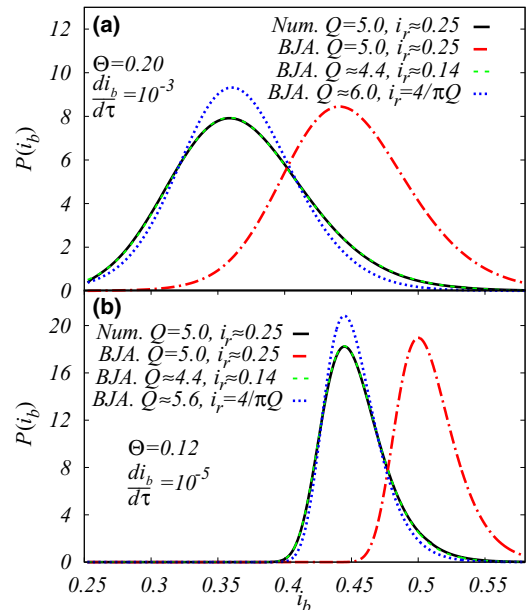


FIG. 5. (Color online) Fitting of retrapping current histograms for two values of the temperature and ramping speed (faster ramping and warmer junction in the upper panel and slower ramp in colder junction in the bottom). Numerically exact solution (full black line) is compared to various fitting procedures based on the BJBMS rate (19): identical junction parameters (red dot-dashed line), both Q and i_r fit (green dashed line), and Q fit while $i_r(Q) \equiv 4/\pi Q$ is constrained (blue dotted line).

less directly the retrapping rate Γ_r . Castellano *et al.* [48] do measure the return (retrapping) current histograms and fit them successfully with the BJBMS formula with 2 fitting parameters: the retrapping current i_r and quality factor Q . In practice, however, these two quantities are related and the retrapping current is a function of the quality factor $i_r(Q)$. This is indeed revealed in the experiment as failing consistency checks comparing the inferred level of dissipation (effectively the quality factor) from the two-parametric histogram fit and from the $i_r(Q)$ relation. This may be an experimental indication of the failure of the BJBMS formula, which clearly would deserve further, more detailed study.

We demonstrate the problem of multiparameter fitting in Fig. 5, where we show results of the various fitting procedures for two values of temperature and ramping rate. The numerically exactly generated retrapping histogram for a moderately damped junction with $Q = 5$ (full black line) is compared with the one generated by the BJBMS rate with identical values of parameters $Q = 5$, $i_r(Q) = 4/\pi Q \approx 0.25$ (red dot-dashed line). Furthermore, the best fits of the exact histogram with the BJBMS formula (19) with both Q and i_r being free fitting parameters (green dashed line) and with Q varying while $i_r(Q) = 4/\pi Q$ constrained (blue dotted line) are plotted. We can see that the BJBMS result with original junction parameters is easily discernible from the exact result. On the other hand, if both parameters are allowed to change and are fit, we see that the exact histogram can be reproduced practically perfectly at the expense of mild modification of the quality factor on the order of 10% but simultaneous

major change in the value of the retrapping current (nearly 50% change compared to reality). This can be understood also from Fig. 4 since the modification of the retrapping current amounts to a corresponding horizontal shift of the curve leading to a nearly perfect overlap of the BJBMS rate with the exact one in a wide upper range of bias currents. This, consequently, leads to a nearly perfect agreement of the switching histograms. However, such a procedure breaks the connection between the $i_r(Q)$ and Q as can be seen from our demonstration: $Q_{\text{fit}} \doteq 4.4$ whereas $Q_{\text{dis}} \equiv 4/\pi i_r \doteq 9.1$ with their ratio exceeding two. We believe that this is similar to the situation in the experiment where a large discrepancy between the two Q values determined by the two procedures was also reported. We also see in Fig. 5 that enforcing the relation $i_r(Q) \equiv 4/\pi Q$ with variable Q leads to some 10% to 20% discrepancy in the fitted histogram as well as the value of the quality factor, which could be possibly distinguishable in the experiment. A new experiment with better characterization of the junction parameters, in particular ideally with an independent characterization of its quality factor, should thus be able to check the (in)validity of the BJBMS approximation as well as our results.

VI. CONCLUSIONS AND OUTLOOK

To summarize, we developed an efficient and reliable numerical scheme based on the matrix continued fraction method for the analysis of phase dynamics in arbitrarily damped current-biased Josephson junctions. It allows us to study the voltage noise and, consequently, analyze in detail various transport regimes, in particular: (a) the regime of multiple phase-slips with their full characterization in terms of the corresponding rates and (b) the switching regime providing us with the escape and retrapping rates. Direct stochastic simulations of these regimes and extracting the corresponding rates is computationally very demanding while our numerics is several orders of magnitude faster. We have studied these rates in detail for moderately damped JJs ($Q \approx 1$ to 10) providing new results in this analytically inaccessible regime. We have checked the consistency of the results and compared our numerical findings with available asymptotic ($Q \rightarrow \infty$) analytical formulas with a good match with Mel'nikov's results [35,36,44]. As a by-product we have clearly identified the very popular and widely used expression for the retrapping rate by Ben-Jacob *et al.* [43] as incorrect which has remained essentially unnoticed due to subtleties of normally employed fitting procedures.

Our prediction for the MPS and retrapping rates can be experimentally verified. In case of MPS the direct verification in JJs might be challenging due to short time extent of the individual phase-slips but the same type of dynamics (RCSJ model) can be realized also in optical tweezers, where the MPS observation should be viable. Retrapping rates can be measured from the switching histogram analysis in the standard JJ setup with down-ramped current bias. Reliable comparison with our theoretical predictions requires using JJs with reasonably frequency-independent damping (in order to justify the RCSJ model) and proper characterization of the junction parameters, in particular the critical current I_c and the retrapping current $I_r(Q)$ (or, equivalently, the quality factor Q)

from an independent measurement(s). Frequency-independent damping occurs in low-resistance superconductor-normal metal-superconductor junctions, which thus obey the RCSJ model [10,46] even though the current-phase relationship may deviate from sinusoidal. That is, however, no problem for our formalism, which yields the retrapping rate for arbitrary current-phase relations and possible deviations from sinusoidal do not influence in any way its reliability or efficiency.

Extensions to more complicated circuits are possible. Arbitrary nonsinusoidal current-phase relations are fully covered by the present formulation as for the mean voltage and voltage noise. Identification of MPS and retrapping regimes requires suitable reformulation if the current-phase relation supports two or more minima within the 2π span of the phase variable, which happens, e.g., in the so-called φ junctions [5]. Extraction of the MPS and escape and retrapping rates then must reflect the existence of multiple nonequivalent locked solutions in the dynamical phase diagram of these exotic JJs. Nevertheless, the procedure can be carried through analogously to the present case, as we will report in a forthcoming publication.

A more serious issue concerns the frequency dependence of the damping which is relevant in particular for conventional small superconductor-insulator-superconductor junctions. Our method cannot be directly applied in this case. However, our results can still be used at least in two ways: The first option uses the fact that simulations of switching experiments such as, e.g., those in Ref. [10], use the switching rates deduced from microscopic dynamics of the RCSJ model as inputs into a ‘‘mesoscopic’’ (or coarse grained) level of description of the switching histograms, which can be successfully modeled this way with the bonus (over the direct fully microscopic stochastic simulations) of gaining more insight and understanding into the physical mechanisms involved. The frequency-dependent damping was included in that work by just two values at low and high frequencies. The rates entering the simulations were still the RCSJ rates for constant damping, just according to their usage the appropriate (i.e., either the low or high frequency) value of the damping was used. Obviously, for such a simulation our method still provides the microscopic rates as essential inputs. Another possibility of applying our formalism to the frequency-dependent damping stems from the fact that the frequency-dependent damping is often modeled by a simple circuit extending the RCSJ model by an RC shunt [9,25]. Under suitable conditions (negligible intrinsic capacitance of the junction) this circuit can be described by a bivariate Fokker-Planck equation [25] analogous (but not identical) to Eq. (3), which can be then solved analogously to the present case by the MCF method. This yields again new numerically exact results for quantities such as the rates for overcoming the so-called dissipation barrier [49], etc. We also defer study of this very interesting problem to another presentation.

Finally, our MCF formalism allows directly for the calculation not only of the zero-frequency but also the finite-frequency noise; see Eq. (8). This may be relevant for the real experiment measuring directly the voltage noise, which would actually couple to finite (though optimally small) frequency-voltage fluctuations. However, this arrangement does not limit the utility of our method for the description of the experimental data.

ACKNOWLEDGMENTS

We thank Pertti Hakonen, Tero Heikkilä, and Gabriel Niebler for stimulating discussions drawing our attention to this problem. We are also very grateful to Edward Goldobin and Pavel Zemánek for advice and very helpful comments on the manuscript. We acknowledge financial support by the Czech Science Foundation via Grant No. 204/11/J042 (M.Ž. and T.N.) and by the Deutsche Forschungsgemeinschaft (DFG, Germany) via BE 3803/5 and SFB 767 (W.B.).

APPENDIX: MATRIX CONTINUED-FRACTION METHOD

In the main text we discuss a numerical solution of the dimensionless Langevin equations (2) with the associated Fokker–Planck equation (3) for the probability distribution function $W(\phi, v, \tau)$. Our first goal is to calculate the mean voltage

$$\langle v \rangle = \int_0^{2\pi} d\phi \int_{-\infty}^{\infty} dv v W_{\text{stat}}(\phi, v), \quad (\text{A1})$$

and the (zero frequency) voltage noise

$$S = \int_{-\infty}^{\infty} d\tau [\langle v(\tau)v(0) \rangle - \langle v(\tau) \rangle \langle v(0) \rangle] \quad (\text{A2})$$

in the stationary state $W_{\text{stat}}(\phi, v) \equiv \lim_{\tau \rightarrow \infty} W(\phi, v; \tau)$ determined by the 2π -periodic solution (in ϕ) of the equation

$$L_{\text{FP}} W_{\text{stat}}(\phi, v) = 0. \quad (\text{A3})$$

We have used the MCF method [3] to obtain the numerical solution for the stationary distribution function and our explanation closely follows that work. The operator L_{FP} can be partitioned into the irreversible L_i and reversible L_r operators reading

$$\begin{aligned} L_i &= \gamma \frac{\partial}{\partial v} \left(v + \Theta \frac{\partial}{\partial v} \right), \\ L_r &= -v \frac{\partial}{\partial \phi} - U'(\phi) \frac{\partial}{\partial v}, \end{aligned} \quad (\text{A4})$$

with the potential

$$U(\phi) = i_b \phi + \cos \phi. \quad (\text{A5})$$

The irreversible operator L_i can be mapped onto the Hamilton operator of the linear harmonic oscillator via a suitable similarity transformation:

$$\tilde{L}_i = \exp \left[\frac{v^2}{4\Theta} \right] L_i \exp \left[-\frac{v^2}{4\Theta} \right] = -\gamma b^\dagger b, \quad (\text{A6})$$

where the creation b^\dagger and annihilation b operators have been introduced

$$\begin{aligned} b^\dagger &= -\sqrt{\Theta} \frac{\partial}{\partial v} + \frac{v}{2\sqrt{\Theta}}, \\ b &= \sqrt{\Theta} \frac{\partial}{\partial v} + \frac{v}{2\sqrt{\Theta}}. \end{aligned} \quad (\text{A7})$$

For the transformed reversible operator we consequently get

$$\tilde{L}_r = \exp \left[\frac{v^2}{4\Theta} \right] L_r \exp \left[-\frac{v^2}{4\Theta} \right] = -b^\dagger D_2 - b D_1, \quad (\text{A8})$$

with ϕ -dependent operators

$$\begin{aligned} D_1 &= \sqrt{\Theta} \frac{\partial}{\partial \phi}, \\ D_2 &= \sqrt{\Theta} \frac{\partial}{\partial \phi} - \frac{U'(\phi)}{\sqrt{\Theta}}. \end{aligned} \quad (\text{A9})$$

Altogether, we have

$$L_{\text{FP}} = \exp \left[-\frac{v^2}{4\Theta} \right] (-\gamma b^\dagger b - b^\dagger D_2 - b D_1) \exp \left[\frac{v^2}{4\Theta} \right]. \quad (\text{A10})$$

After these manipulations it is convenient to expand the v -dependent part of distribution function $W(\phi, v; \tau)$ into the linear-harmonic-oscillator eigenfunctions $\psi_n(v)$

$$W(\phi, v; \tau) = \psi_0(v) \sum_n c_n(\phi; \tau) \psi_n(v), \quad (\text{A11})$$

given by (with $\kappa = 1/\sqrt{2\Theta}$)

$$\begin{aligned} \psi_0(v) &= \frac{e^{-\frac{(\kappa v)^2}{2}}}{\sqrt{\kappa\sqrt{\pi}}}, \\ \psi_n(v) &= \frac{(b^\dagger)^n}{\sqrt{n!}} \psi_0(v), \end{aligned} \quad (\text{A12})$$

or in terms of the Hermite polynomials $H_n(x)$,

$$\psi_n(v) = \frac{H_n(\kappa v) e^{-\frac{(\kappa v)^2}{2}}}{\sqrt{n! 2^n \kappa \sqrt{\pi}}}. \quad (\text{A13})$$

The oscillator functions are the eigenfunctions of the irreversible part of the L_{FP} operator and with the correct boundary conditions $\lim_{v \rightarrow \pm\infty} W(\phi, v; \tau) = 0$. Consequently,

$$\int_{-\infty}^{\infty} dv W(\phi, v; \tau) = c_0(\phi; \tau), \quad (\text{A14})$$

$$\int_{-\infty}^{\infty} dv v W(\phi, v; \tau) = \sqrt{\Theta} c_1(\phi; \tau), \quad (\text{A15})$$

and the ϕ -dependent coefficients $c_n(\phi; \tau)$ read

$$c_n(\phi; \tau) = \int_{-\infty}^{\infty} dv \psi_n(v) W(\phi, v; \tau) / \psi_0(v). \quad (\text{A16})$$

Using Eqs. (A6)–(A11) we can construct the Brinkman hierarchy equivalent to the Fokker–Planck equation (3):

$$\begin{aligned} \frac{\partial}{\partial \tau} c_m(\phi; \tau) &= -\sqrt{m} D_2 c_{m-1}(\phi; \tau) - \gamma m c_m(\phi; \tau) \\ &\quad - \sqrt{m+1} D_1 c_{m+1}(\phi; \tau). \end{aligned} \quad (\text{A17})$$

1. Stationary Distribution and Mean Voltage

Because of the chosen potential (A5) the Fokker–Planck operator (A10) commutes with the translation operator T defined by

$$T W(\phi, v; \tau) \equiv W(\phi + 2\pi, v; \tau), \quad (\text{A18})$$

and, therefore, the eigenfunctions $\varphi_n(k, \phi, v)$ of operator L_{FP} and its adjoint operator L_{FP}^+

$$\begin{aligned} L_{\text{FP}}\varphi_n(k, \phi, v) &= \lambda_n(k)\varphi_n(k, \phi, v), \\ L_{\text{FP}}^+\varphi_n^+(k, \phi, v) &= \lambda_n(k)\varphi_n^+(k, \phi, v), \end{aligned} \quad (\text{A19})$$

with $k \in (-1/2, 1/2]$ restricted to the first Brillouin zone can be written in the form of the Bloch waves:

$$\begin{aligned} \varphi_n(k, \phi, v) &= e^{-ik\phi} u_n(k, \phi, v), \\ u_n(k, \phi, v) &= u_n(k, \phi + 2\pi, v), \\ \varphi_n^+(k, \phi, v) &= e^{ik\phi} u_n^+(k, \phi, v), \\ u_n^+(k, \phi, v) &= u_n^+(k, \phi + 2\pi, v). \end{aligned} \quad (\text{A20})$$

Consequently, the solutions of the Eq. (A3) can be chosen to be

$$W_{\text{stat}}(\phi, v) = e^{-ik\phi} u(k, \phi, v), \quad (\text{A21})$$

with $e^{-i2\pi k}$ ($-1/2 < k \leq 1/2$) being the eigenvalues of the translation operator T . The stationary expansion coefficients $c_n(\phi) \equiv \lim_{\tau \rightarrow \infty} c_n(\phi; \tau)$ must thus have the form

$$c_n(\phi) = e^{-ik\phi} u_n(k, \phi), \quad u_n(k, \phi) = u_n(k, \phi + 2\pi). \quad (\text{A22})$$

Note that the stationary form of the Brinkman hierarchy (A17) reads

$$\begin{aligned} \sqrt{1}D_1c_1(\phi) &= 0, \\ \sqrt{1}D_2c_0(\phi) + 1\gamma c_1(\phi) + \sqrt{2}D_1c_2(\phi) &= 0, \\ \sqrt{2}D_2c_1(\phi) + 2\gamma c_2(\phi) + \sqrt{3}D_1c_3(\phi) &= 0, \\ &\vdots \end{aligned} \quad (\text{A23})$$

from which it is obvious that $c_1(\phi) = c_1 = \text{const}$. Since c_1 is related by Eq. (A15) to the mean voltage being generically nonzero, the constancy of c_1 implies $k = 0$ for the stationary solution. Thus, the stationary distribution function is periodic

$$W_{\text{stat}}(\phi, v) = W_{\text{stat}}(\phi + 2\pi, v), \quad c_n(\phi) = c_n(\phi + 2\pi) \quad (\text{A24})$$

and can be normalized in one period:

$$\int_0^{2\pi} d\phi \int_{-\infty}^{\infty} dv W_{\text{stat}}(\phi, v) = \int_0^{2\pi} d\phi c_0(\phi) = 1, \quad (\text{A25})$$

$$\begin{aligned} \langle v \rangle &= \int_0^{2\pi} d\phi \int_{-\infty}^{\infty} dv v W_{\text{stat}}(\phi, v) \\ &= \sqrt{\Theta} \int_0^{2\pi} d\phi c_1(\phi) = \sqrt{\Theta} 2\pi c_1. \end{aligned} \quad (\text{A26})$$

To solve Eq. (A3) for the periodic coefficients $c_m(\phi)$ we have used the Fourier series expansion

$$c_m(\phi) = \frac{1}{\sqrt{2\pi}} \sum_{p \in \mathbb{Z}} c_m^p e^{ip\phi}, \quad (\text{A27})$$

allowing us to define the matrix elements of operators $\mathcal{D}_m^+, \mathcal{D}_m, \mathcal{D}_m^-$:

$$\begin{aligned} (\mathcal{D}_m^+)^{pq} &\equiv -\frac{\sqrt{m+1}}{2\pi} \int_0^{2\pi} d\phi e^{-ip\phi} D_1 e^{iq\phi} \\ &= -i\sqrt{m+1}\sqrt{\Theta} p \delta_{p,q}, \end{aligned}$$

$$(\mathcal{D}_m)^{pq} \equiv -\gamma m \delta_{p,q}, \quad (\text{A28})$$

$$\begin{aligned} (\mathcal{D}_m^-)^{pq} &\equiv -\frac{\sqrt{m}}{2\pi} \int_0^{2\pi} d\phi e^{-ip\phi} D_2 e^{iq\phi} \\ &= -i\sqrt{m}\sqrt{\Theta} \left[\left(p + i\frac{i_b}{\Theta} \right) \delta_{p,q} + \frac{\delta_{p,q-1} - \delta_{p,q+1}}{2\Theta} \right], \end{aligned}$$

which can be used to recast Eq. (A23) into the form of a vector tridiagonal recurrence relation

$$\mathcal{D}_m^- \mathbf{c}_{m-1} + \mathcal{D}_m \mathbf{c}_m + \mathcal{D}_m^+ \mathbf{c}_{m+1} = 0, \quad (\text{A29})$$

where \mathbf{c}_m is a time-independent vector of expansion coefficients c_m^p from Eq. (A27)

$$\mathbf{c}_m = \begin{pmatrix} \vdots \\ c_m^{-1} \\ c_m^0 \\ c_m^1 \\ \vdots \end{pmatrix}. \quad (\text{A30})$$

For solving relation (A29) we have defined matrices \mathcal{S}_m obeying

$$\mathbf{c}_{m+1} = \mathcal{S}_m \mathbf{c}_m, \quad \mathbf{c}_m = \mathcal{S}_m^{-1} \mathbf{c}_{m+1}, \quad (\text{A31})$$

which transforms Eq. (A29) into

$$\mathcal{D}_m^- \mathcal{S}_{m-1}^{-1} \mathbf{c}_m + \mathcal{D}_m \mathbf{c}_m + \mathcal{D}_m^+ \mathcal{S}_m \mathbf{c}_m = 0, \quad (\text{A32})$$

and, consequently, a matrix continued-fraction structure can be constructed:

$$\mathcal{S}_{m-1} = -(\mathcal{D}_m + \mathcal{D}_m^+ \mathcal{S}_m)^{-1} \mathcal{D}_m^-. \quad (\text{A33})$$

By truncating the recurrence at $m = M$, i.e., setting $\mathbf{c}_{m>M} \equiv 0$ in Eq. (A29) and using the normalization condition (A25), together with the fact that the coefficient c_1 is constant we obtain for the vector \mathbf{c}_0

$$c_0^p = \frac{1}{\sqrt{2\pi}} \frac{(\mathcal{S}_0^{-1})^{p0}}{(\mathcal{S}_0^{-1})^{00}}. \quad (\text{A34})$$

All other vectors \mathbf{c}_m follow from Eq. (A31). In particular, the average voltage reads

$$\langle v \rangle = \sqrt{\Theta} 2\pi c_1 \equiv \sqrt{2\pi \Theta} c_1^0 = \frac{\sqrt{\Theta}}{(\mathcal{S}_0^{-1})^{00}}. \quad (\text{A35})$$

2. Voltage noise

We obtained the numerical solution of Eq. (10) analogously to the solution of Eq. (A3)—the main difference is that, for Eq. (10), the vector tridiagonal recurrence relation has a right-hand side

$$\mathcal{D}_m^- \mathbf{a}_{m-1} + \mathcal{D}_m \mathbf{a}_m + \mathcal{D}_m^+ \mathbf{a}_{m+1} = \boldsymbol{\alpha}_m, \quad (\text{A36})$$

with \mathbf{a}_m being a time-independent vector of expansion coefficients a_m^p of $R(\phi, v)$ obtained in the same procedure as for coefficients c_m^p in Eq. (A27) for $W_{\text{stat}}(\phi, v)$ and

$$\boldsymbol{\alpha}_m = \sqrt{\Theta} m \mathbf{c}_{m-1} - \langle v \rangle \mathbf{c}_m + \sqrt{\Theta(m+1)} \mathbf{c}_{m+1}. \quad (\text{A37})$$

Introducing the correction vectors \mathbf{g}_m satisfying

$$\mathbf{a}_{m+1} = \mathcal{S}_m \mathbf{a}_m + \mathbf{g}_m, \quad (\text{A38})$$

Eq. (A36) gives a recurrent prescription for their evaluation

$$\mathbf{g}_{m-1} = -(\mathcal{D}_m + \mathcal{D}_m^+ \mathcal{S}_m)^{-1} (\mathcal{D}_m^+ \mathbf{g}_m - \boldsymbol{\alpha}_m). \quad (\text{A39})$$

After truncation of Eq. (A36) at $m = M$ and using the proper normalization conditions together with Eq. (A38) this recurrent relation is used to obtain the auxiliary quantity $R(\phi, v)$ and, consequently, the voltage noise.

3. Nonstationary solution

Because we are interested in the statistics of $2\pi n$ phase-slips we have to consider also nonperiodic solutions of the Fokker–Planck equation in the nonstationary case. Recalling the expansion Eq. (A11) and the Brinkman hierarchy Eq. (A17) it is clear that in order to make use of the MCF method we need a complete set of functions $\varphi^p(\phi)$ in which the coefficients $c_m(\phi; \tau)$ can be expanded. One of the possibilities is to use the eigenfunctions Eq. (A20) or, equivalently, make use of the Floquet theorem as an ansatz for the nonperiodic solution,

$$W(\phi, v; \tau) = \int_{-\frac{1}{2}}^{\frac{1}{2}} dk \mathcal{W}(k, \phi, v; \tau) e^{-ik\phi}, \quad (\text{A40})$$

where $\mathcal{W}(k, \phi, v; \tau)$ is periodic in ϕ with period 2π and k is again restricted to the first Brillouin zone. Similarly as done before for the distribution function, the function $\mathcal{W}(k, \phi, v; \tau)$ can be expanded in

$$\mathcal{W}(k, \phi, v; \tau) = \psi_0(v) \sum_n \sum_p c_n^p(k; \tau) e^{ip\phi} \psi_n(v), \quad (\text{A41})$$

yielding the complete set of functions

$$\varphi^p(k, \phi) = \frac{1}{\sqrt{2\pi}} e^{i(p-k)\phi}, \quad (\text{A42})$$

in which the coefficients $c_m(\phi; \tau)$ are expanded. Using time-dependent vectors $\mathbf{c}_m(k; \tau)$ of expansion coefficients $c_m^p(k; \tau)$, Eq. (A29) changes to

$$\mathcal{D}_m^- \mathbf{c}_{m-1}(k; \tau) + \mathcal{D}_m \mathbf{c}_m(k; \tau) + \mathcal{D}_m^+ \mathbf{c}_{m+1}(k; \tau) = \dot{\mathbf{c}}_m(k; \tau), \quad (\text{A43})$$

with

$$\begin{aligned} (\mathcal{D}_m^+)^{pq} &= -\frac{\sqrt{m+1}}{2\pi} \int_0^{2\pi} d\phi e^{-i(p-k)\phi} \mathcal{D}_1 e^{i(p-k)\phi} \\ &= -i\sqrt{m+1} \sqrt{\Theta} (p-k) \delta_{p,q}, \\ (\mathcal{D}_m)^{pq} &= -\gamma m \delta_{p,q}, \\ (\mathcal{D}_m^-)^{pq} &= -\frac{\sqrt{m}}{2\pi} \int_0^{2\pi} d\phi e^{-i(p-k)\phi} \mathcal{D}_2 e^{i(p-k)\phi} \\ &= -i\sqrt{m} \sqrt{\Theta} \left[\left(p-k + i \frac{i_b}{\Theta} \right) \delta_{p,q} \right. \\ &\quad \left. + \frac{\delta_{p,q-1} - \delta_{p,q+1}}{2\Theta} \right]. \end{aligned} \quad (\text{A44})$$

One way to solve this initial-value problem is to use the Laplace transform

$$\tilde{\mathbf{c}}_m(k; s) = \int_0^\infty d\tau \mathbf{c}_m(k; \tau) e^{-s\tau}, \quad (\text{A45})$$

which turns Eq. (A43) into

$$\mathcal{D}_m^- \tilde{\mathbf{c}}_{m-1}(k; s) + \tilde{\mathcal{D}}_m \tilde{\mathbf{c}}_m(k; s) + \mathcal{D}_m^+ \tilde{\mathbf{c}}_{m+1}(k; s) = -\mathbf{c}_m(k; 0), \quad (\text{A46})$$

with

$$\tilde{\mathcal{D}}_m \equiv \mathcal{D}_m - sI. \quad (\text{A47})$$

This equation can be solved analogously to the solution of Eq. (A36) and the resulting s -dependent quantities can be inverse Laplace transformed to the time domain. Alternatively, one can use the homogeneous version of Eq. (A46) for determining the eigenvalues of the Fokker–Planck operator from the condition

$$\text{Det}[\mathcal{D}_m - \lambda I + \mathcal{D}_m^- \mathcal{S}_{m-1}^{-1}(\lambda) + \mathcal{D}_m^+ \mathcal{S}_m(\lambda)] = 0 \quad (\text{A48})$$

and, consequently, for finding the nonstationary solution by the spectral decomposition

$$W(\phi, v; \tau) = \int_{-1/2}^{1/2} dk \sum_n e^{-ik\phi} u_n(k, \phi, v) e^{\lambda_n(k)\tau}. \quad (\text{A49})$$

The advantage of the eigenfunction expansion is that the transition probability from state ϕ', v' to ϕ, v has the simple form (Ref. [3, Sec. 11.7])

$$\begin{aligned} P(\phi, v; \tau | \phi', v', 0) &= \int_{-1/2}^{1/2} dk \sum_n u_n^+(k, \phi', v') u_n(k, \phi, v) \\ &\quad \times e^{-ik(\phi-\phi')} e^{\lambda_n(k)\tau}, \end{aligned} \quad (\text{A50})$$

whose long-time asymptotics is easily determined as [we assume that the eigenvalue $\lambda_0(k)$ with the highest real part corresponding to the stationary solution with $\lambda_0(0) = 0$ is separated by a finite gap from other eigenvalues $\text{Re}[\lambda_n(k) - \lambda_0(k)] < 0$ for $n \geq 1$]

$$\begin{aligned} P(\phi, v; \tau \rightarrow \infty | \phi', v', 0) &\approx \int_{-1/2}^{1/2} dk u_0^+(k, \phi', v') u_0(k, \phi, v) e^{-ik(\phi-\phi')} e^{\lambda_0(k)\tau}, \end{aligned} \quad (\text{A51})$$

or

$$W(\phi, v; \tau \rightarrow \infty) = \int_{-1/2}^{1/2} dk I_0(k) u_0(k, \phi, v) e^{-ik\phi} e^{\lambda_0(k)\tau}, \quad (\text{A52})$$

with $I_0(k)$ being determined solely by the initial condition.

4. Full Counting Statistics

As pointed out in the end of Sec. II an alternative method for the evaluation of the voltage cumulants is to use the full counting statistics (FCS) approach pioneered in this context in Ref. [20]. The aim of that method is the calculation of the k -dependent (k is the *counting field*) cumulant generating function (CGF) $F(k; \tau) \equiv \ln \int_{-\infty}^{\infty} d\phi e^{ik\phi} \int_{-\infty}^{\infty} dv W(\phi, v; \tau)$ from a nonstationary solution $W(\phi, v; \tau)$ of Eq. (3) (Ref. [3, Sec. 11.7]). Using the Floquet theorem and Eq. (A52) once again

the CGF can be written as

$$\begin{aligned}
\exp[F(k; \tau \rightarrow \infty)] &\equiv \int_{-\infty}^{\infty} d\phi \int_{-\infty}^{\infty} dv W(\phi, v; \tau \rightarrow \infty) e^{ik\phi} \\
&\approx \int_{-\infty}^{\infty} d\phi \int_{-\infty}^{\infty} dv \int_{-\frac{1}{2}}^{\frac{1}{2}} dl I_0(l) u_0(l, \phi, v) e^{\lambda_0(l)\tau} e^{i(k-l)\phi} \\
&= \frac{1}{\sqrt{2\pi}} \int_{-\infty}^{\infty} d\phi \int_{-\frac{1}{2}}^{\frac{1}{2}} dl I_0(l) \sum_p c_0^p(l) e^{i(p-l+k)\phi} e^{\lambda_0(l)\tau} \\
&= \frac{1}{\sqrt{2\pi}} \int_{-\frac{1}{2}}^{\frac{1}{2}} dl I_0(l) e^{\lambda_0(l)\tau} \sum_p c_0^p(l) \lim_{N \rightarrow \infty} \sum_{n=-N}^N \left\{ \int_{2\pi n}^{2\pi(n+1)} d\phi e^{i(p-l+k)\phi} \right\} \\
&= \frac{1}{\sqrt{2\pi}} \int_{-\frac{1}{2}}^{\frac{1}{2}} dl I_0(l) e^{\lambda_0(l)\tau} \sum_p c_0^p(l) \int_0^{2\pi} d\phi e^{i(p-l+k)\phi} \lim_{N \rightarrow \infty} \sum_{n=-N}^N e^{2\pi i(p-l+k)n} \\
&= \frac{1}{\sqrt{2\pi}} \int_{-\frac{1}{2}}^{\frac{1}{2}} dl I_0(l) e^{\lambda_0(l)\tau} \sum_p c_0^p(l) \Xi(p-l+k) \int_0^{2\pi} d\phi e^{i(p-l+k)\phi}. \tag{A53}
\end{aligned}$$

As both l and k are from the first Brillouin zone and p is an integer the use of the Dirac comb function $\Xi(x) = \sum_{n \in \mathbb{Z}} \delta(x-n)$ implies $p=0$ and $k=l$ which leads to

$$F(k; \tau \rightarrow \infty) = \lambda_0(k)\tau + \ln \sqrt{2\pi} I_0(k) c_0^0(k). \tag{A54}$$

The second term depends on the initial state of the system and is irrelevant in the long-time limit. The zero-frequency n th cumulant of v follows from [20]

$$C_n = \lim_{\tau \rightarrow \infty} \frac{(-i)^n}{\tau} \frac{\partial^n F(k, \tau)}{\partial k^n} \Big|_{k=0} = (-i)^n \frac{\partial^n \lambda_0(k)}{\partial k^n} \Big|_{k=0}. \tag{A55}$$

-
- [1] A. Barone and G. Paternò, *Physics and Applications of the Josephson Effect* (A Willey-Interscience Publications, John Wiley & Sons, New York, Chichester, Brisbane, Toronto, Singapore, 1982); K. K. Likharev, *Dynamics of Josephson Junctions and Circuits* (Gordon and Breach, New York, 1986).
- [2] R. L. Kautz, *Rep. Prog. Phys.* **59**, 935 (1996).
- [3] H. Risken, *The Fokker-Planck Equation*, 2nd ed. (Springer-Verlag, Berlin, Heidelberg, 1989).
- [4] A. I. Buzdin, *Rev. Mod. Phys.* **77**, 935 (2005).
- [5] H. Sickinger, A. Lipman, M. Weides, R. G. Mints, H. Kohlstedt, D. Koelle, R. Kleiner, and E. Goldobin, *Phys. Rev. Lett.* **109**, 107002 (2012).
- [6] S. De Franceschi, L. Kouwenhoven, C. Schönberger, and W. Wernsdorfer, *Nat. Nanotechnol.* **5**, 703 (2010).
- [7] E. Goldobin, R. Kleiner, D. Koelle, and R. G. Mints, *Phys. Rev. Lett.* **111**, 057004 (2013).
- [8] J. M. Martinis and R. L. Kautz, *Phys. Rev. Lett.* **63**, 1507 (1989).
- [9] R. L. Kautz and J. M. Martinis, *Phys. Rev. B* **42**, 9903 (1990).
- [10] J. C. Fenton and P. A. Warburton, *Phys. Rev. B* **78**, 054526 (2008).
- [11] L. I. McCann, M. Dykman, and B. Golding, *Nature (London)* **402**, 785 (1999).
- [12] S. A. Tatarkova, W. Sibbett, and K. Dholakia, *Phys. Rev. Lett.* **91**, 038101 (2003).
- [13] T. Čížmár, M. Šiler, M. Šerý, P. Zemánek, V. Garcés-Chávez, and K. Dholakia, *Phys. Rev. B* **74**, 035105 (2006).
- [14] M. Šiler, T. Čížmár, A. Jonáš, and P. Zemánek, *New J. Phys.* **10**, 113010 (2008).
- [15] M. Šiler and P. Zemánek, *New J. Phys.* **12**, 083001 (2010).
- [16] O. Brzobohatý, M. Šiler, J. Ježek, P. Ják, and P. Zemánek, *Opt. Lett.* **38**, 4601 (2013).
- [17] J. Gieseler, L. Novotny, and R. Quidant, *Nat. Phys.* **9**, 806 (2013).
- [18] T. Li, S. Kheifets, and M. G. Raizen, *Nat. Phys.* **7**, 527 (2011).
- [19] R. F. Voss, *J. Low Temp. Phys.* **42**, 151 (1981).
- [20] D. S. Golubev, M. Marthaler, Y. Utsumi, and G. Schön, *Phys. Rev. B* **81**, 184516 (2010).
- [21] M. Žonda and T. Novotný, *Phys. Scr. T* **151**, 014023 (2012).
- [22] P. Hakonen, private communication.
- [23] M. Vanević, Y. V. Nazarov, and W. Belzig, *Phys. Rev. Lett.* **99**, 076601 (2007); *Phys. Rev. B* **78**, 245308 (2008); C. Padurariu, F. Hassler, and Y. V. Nazarov, *ibid.* **86**, 054514 (2012).
- [24] J. Basset, R. Delagrè, R. Weil, A. Kasumov, H. Bouchiat, and R. Deblock, *J. Appl. Phys.* **116**, 024311 (2014).
- [25] P. Joyez, D. Vion, M. Götz, M. Devoret, and D. Esteve, *J. Supercond.* **12**, 757 (1999).
- [26] C. H. Webster, J. C. Fenton, T. T. Hongisto, S. P. Giblin, A. B. Zorin, and P. A. Warburton, *Phys. Rev. B* **87**, 144510 (2013).
- [27] D. E. McCumber, *J. Appl. Phys.* **39**, 3113 (1968); W. C. Stewart, *Appl. Phys. Lett.* **12**, 277 (1968).
- [28] C. Flindt, T. Novotný, and A.-P. Jauho, *Phys. Rev. B* **70**, 205334 (2004).
- [29] C. Flindt, T. Novotný, and A.-P. Jauho, *Phys. E (Amsterdam, Neth.)* **29**, 411 (2005).
- [30] D. A. Bagrets and Y. V. Nazarov, *Phys. Rev. B* **67**, 085316 (2003).

- [31] C. Flindt, T. Novotný, and A.-P. Jauho, *Europhys. Lett.* **69**, 475 (2005).
- [32] Despite the seeming simplicity of this task, there are nontrivial aspects being addressed even nowadays—see, e.g., Ref. [50].
- [33] Y. M. Blanter and M. Büttiker, *Phys. Rep.* **336**, 1 (2000).
- [34] C. Beenakker and C. Schönberger, *Phys. Today* **56**(5), 37 (2003).
- [35] V. I. Mel'nikov, *Zh. Eksp. Teor. Fiz.* **88**, 1429 (1985).
- [36] V. I. Mel'nikov, *Phys. Rep.* **209**, 1 (1991).
- [37] By multiple phase-slips we mean here thermally activated changes of the phase-difference variable by an integer multiple of 2π in the sense of Ref. [51].
- [38] K. J. Challis and M. W. Jack, *Phys. Rev. E* **87**, 052102 (2013).
- [39] H. A. Kramers, *Physica* **7**, 284 (1940).
- [40] P. Hänggi, P. Talkner, and M. Borkovec, *Rev. Mod. Phys.* **62**, 251 (1990).
- [41] A. I. Shushin, *Europhys. Lett.* **60**, 525 (2002); *Chem. Phys.* **370**, 244 (2010).
- [42] A. N. Jordan and E. V. Sukhorukov, *Phys. Rev. Lett.* **93**, 260604 (2004).
- [43] E. Ben-Jacob, D. J. Bergman, B. J. Matkowsky, and Z. Schuss, *Phys. Rev. A* **26**, 2805 (1982).
- [44] V. I. Mel'nikov, *Zh. Eksp. Teor. Fiz.* **93**, 2037 (1987).
- [45] P. Jung and H. Risken, *Z. Phys. B: Condens. Matter* **54**, 357 (1984).
- [46] J. Männik, S. Li, W. Qiu, W. Chen, V. Patel, S. Han, and J. E. Lukens, *Phys. Rev. B* **71**, 220509 (2005); V. M. Krasnov, T. Bauch, S. Intiso, E. Hürfeld, T. Akazaki, H. Takayanagi, and P. Delsing, *Phys. Rev. Lett.* **95**, 157002 (2005); J. M. Kivioja, T. E. Nieminen, J. Claudon, O. Buisson, F. W. J. Hekking, and J. P. Pekola, *ibid.* **94**, 247002 (2005); V. M. Krasnov, T. Golod, T. Bauch, and P. Delsing, *Phys. Rev. B* **76**, 224517 (2007); A. Murphy, P. Weinberg, T. Aref, U. C. Coskun, V. Vakaryuk, A. Levchenko, and A. Bezryadin, *Phys. Rev. Lett.* **110**, 247001 (2013).
- [47] R. L. Kautz, *Phys. Rev. A* **38**, 2066 (1988).
- [48] M. G. Castellano, G. Torrioli, F. Chiarello, C. Cosmelli, and P. Carelli, *J. Appl. Phys.* **86**, 6405 (1999).
- [49] D. Vion, M. Götz, P. Joyez, D. Esteve, and M. H. Devoret, *Phys. Rev. Lett.* **77**, 3435 (1996).
- [50] M. V. Fistul, Josephson phase diffusion in small Josephson junctions: a strongly nonlinear regime, [arXiv:1405.1876](https://arxiv.org/abs/1405.1876).
- [51] W. A. Little, *Phys. Rev.* **156**, 396 (1967).